Determination of Acoustic Impedance for Helmholtz Resonators Through Incompressible Unsteady Flow Simulations

J. Tournadre*

Siemens Industry Software, 3001 Leuven, Belgium

K. Förner[†] and W. Polifke[‡]

Technical University of Munich, 85748 Garching bei München, Germany

P. Martínez-Lera[§]

Siemens Industry Software, 3001 Leuven, Belgium

and

W. Desmet[¶]

KU Leuven, 3001 Leuven, Belgium

The present work proposes and assesses a methodology based on incompressible computational fluid dynamics simulations to study the acoustic behavior of Helmholtz resonators under a large range of excitation amplitudes. It constitutes an alternative approach to the more widespread one based on compressible flow simulations to analyze the nonlinear regime of Helmholtz resonators. In the present methodology, the resonator is decomposed into its two main components: an assumed incompressible orifice neck and a compressible backing volume. The transfer impedance of the single orifice is obtained by means of an incompressible solver of the flow equations without turbulence modeling, whereas an analytical model accounts for the compliance of the gas in the backing cavity. The proposed methodology is compared for validation purposes to both numerical results of the full compressible equations and experimental data for the complete resonator at different sound pressure levels. A good agreement between the results of the two numerical approaches could be achieved. Numerical results match also fairly well with experimental data, but a systematic overprediction of the resistance by simulations is observed. Accounting for the presence of microrounded edges, presumably present due to manufacturing processes, allows a better agreement between numerical and experimental results.

Nomenclature

$A_f, A_{f,o}$	=	input amplitudes for compressible simulations, m/s
A_u	=	input amplitudes for incompressible simulations, m/s
c	=	speed of sound, m/s
d_{cav}	=	back-cavity diameter, m
d_o	=	orifice diameter, m
F_r, G_r	=	Riemann invariants, m/s
$f_{H,lin}$	=	Helmholtz resonance frequency in linear regime, Hz
He	=	Helmholtz number
l_o	=	orifice thickness, m
l_{cav}	=	back-cavity length, m
P	=	total pressure, Pa
p	=	pressure, Pa
$R_{exp/num}$	=	reflection coefficient
$S_{o/bc}$	=	orifice/back-cavity cross-sectional area, m^2
Sh	=	Shear number
u'	=	fluctuating velocity in duct, m/s
u_o'	=	fluctuating velocity in orifice, m/s
Z	=	acoustic impedance, (Pa · s)/m
z	=	normalized acoustic impedance
Δp	=	pressure loss, Pa
λ_a	=	acoustic wavelength, m
ρ	=	density, kg/m^3
σ	=	open area ratio
ϕ	=	acoustic velocity potential, m^2/s
Ω	=	vorticity, m^{-1}

Superscripts

$\hat{\bullet}$	=	Fourier transformed variable
$\bullet'$	=	time fluctuating quantity

I. Introduction

ACOUSTIC damping systems, such as Helmholtz resonators, perforated liners, and quarter-wavelength cavities, are commonly used in multiple industrial applications to reduce sound transmission and to control acoustic feedback that can lead to instabilities, for instance, in combustion systems like aeroengines or gas turbines. When designed properly, such devices dissipate the acoustic energy at a specific bandwidth. The behavior of such an acoustic damper is often characterized by its acoustic impedance, which is defined in the frequency domain as the ratio of the pressure to the normal acoustic velocity. The acoustic dissipation mechanisms, and therefore the impedance values, differ significantly depending on the amplitude of the acoustic excitation. For low excitation amplitudes, the viscous dissipation dominates. In this case, the impedance is independent of the sound amplitude, and the resonator or orifice behaves like a linear system. Numerical methods based on linearized equations, like the linearized Navier–Stokes equations, allow for an efficient treatment of this linear regime with limited computational costs [1]. By increasing the excitation amplitudes, nonlinear effects appear and become progressively dominant. Such nonlinear effects originate from flow

separation at the neck of the resonator, which transfers acoustic energy to the hydrodynamic field. The creation of vortices at the orifice neck increases considerably the dissipation of the acoustic energy. This feature is of importance for the design of acoustic dampers, as it impacts substantially the sound wave attenuation. The nonlinear regime is, however, more complex to predict accurately due to the intricate nature of the physical phenomena taking place. Linear numerical methods are therefore not suitable at medium and high excitation amplitudes, and nonlinear time domain solvers are needed.

The present work investigates the capability of an incompressible unsteady computational fluid dynamic approach to study numerically the aeroacoustic response of a Helmholtz resonator to an external acoustic excitation. Different sound pressure levels (SPLs) are included in this study to cover the different regimes of an investigated Helmholtz resonator. Incompressible flow computations have already successfully been used in the past to characterize the acoustic behavior of confined flow systems. In the work of Martínez-Lera et al. [2], an approach combining incompressible computational fluid dynamics (CFD) and vortex sound theory [3] was applied successfully to a two-dimensional laminar flow through a T joint. This methodology was further improved and applied to corrugated pipes by Nakiboğlu [4] and to a large orifice configuration with through flow by Lacombe et al. [5] for whistling prediction. In contrast to those previous works, the present study focuses on both linear and nonlinear regimes of Helmholtz resonators in the absence of mean flow. The extension to the case with flow can be done easily due to the present general formulation and arguments presented by Nakiboğlu [4] and Golliard et al. [6].

Section II explains in detail the methodology applied here for the numerical acoustic characterization of a Helmholtz resonator. The numerical setup and the postprocessing steps used to determine the surface impedance of the resonator are described. In Secs. III and IV, the results for the impedance describing functions estimated by the proposed approach are shown for the linear and nonlinear regimes, respectively. In both cases, the results are compared to impedance values obtained using compressible flow computation of the complete resonator and validated against measurements data. Section V concludes this paper with an overview of the main observations of this study.

II. Description of Methodology and Case Study

A. Decomposed Helmholtz Resonator

The basic idea of using an incompressible solver to study the acoustic behavior of a Helmholtz resonator, placed at the termination of a duct as depicted in Fig. 1a, appears as a contradiction at first thought. The incompressible nature of the fluid violates indeed the principle of mass conservation if a nonzero inlet velocity is prescribed at the open side of the duct closed by the resonator, which makes impossible the direct study of this configuration by incompressible CFD simulation. The methodology proposed here to face this issue is to decompose the complete Helmholtz resonator into its two main components: the orifice neck and the backing cavity (see Fig. 1b). Such a decomposition has already been proposed by Ingard and Ising [7]. For most of the configurations of interest, the orifice can

be considered acoustically compact; i.e., the Helmholtz number He, which describes the ratio of the neck length or diameter to the acoustic wavelength λ_a, is small ($He \ll 1$). Thus, the flow through the orifice can be treated as incompressible. The compressible effects occur solely in the backing volume. The orifice transfer impedance Z_o is often used to quantify the acoustic behavior of an orifice. It is defined as the ratio of the Fourier component (superscript $\hat{}$) of the fluctuating pressure drop $\Delta \hat{p}' = \hat{p}'_1 - \hat{p}'_2$ and velocity normal to the reference surface in the duct front of the resonator u', i.e.,

$$Z_o = \frac{\Delta \hat{p}'}{\hat{u}'} \tag{1}$$

Note that in the previous definition the velocity $\hat{u}'$ is the cross-sectional surface averaged velocity in the resonance tube. There are other authors using the cross-sectional surface averaged velocity in the orifice u'_o instead. These two velocities are related via the porosity of the resonator plate σ, such that $u' = \sigma u'_o$. The porosity is defined as $\sigma = S_o/S_{bc}$, with S_o and S_{bc} denoting the cross-sectional areas of the orifice and backing cavity, respectively.

The contribution of the backing volume can be described in terms of a surface impedance, $Z_{bc} = \hat{p}'_2/\hat{u}'_2$, which is done here analytically, as described in Sec. II.A.2. The orifice transfer impedance can therefore be expressed as

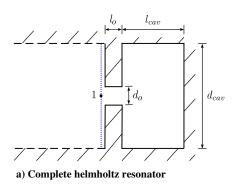$$Z_o = \frac{\hat{p}'_1 - Z_{bc}\hat{u}'_2}{\hat{u}'_1} \tag{2}$$

Because of the acoustically compact neck and the same areas on both sides of the orifice, it is reasonable to assume $\hat{u}'_1 = \hat{u}'_2$. Thus, the surface impedance of the resonator Z_r is given in this lumped model as (cf. Ingard and Ising [7])
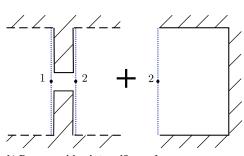
$$Z_r = Z_o + Z_{bc} \tag{3}$$

The present study builds on this Helmholtz resonator decomposition and aims to investigate the validity of this decomposition at different levels of sound excitation. In doing so, the advantages of an incompressible solver are exploited for the simulation of the flow through the orifice, including the vortex generation responsible for the nonlinear acoustic losses. Details on the estimation of the orifice transfer impedance and backing volume surface impedance are given in the following sections.

1. Orifice Impedance Z_o

The methodology to get the orifice transfer impedance from the incompressible simulations is explained in this section. In the plane wave regime, a one-dimensional approximation along the duct is possible, and the area-averaged absolute pressure at several sections of the duct is stored at each time step of the flow simulation. This allows computing the pressure differences between two arbitrarily chosen sections separated by the orifice: $\Delta p_{AB} = p_A - p_B$ is the pressure jump (or loss) between the sections A on the inlet side and B on the outlet side (see Fig. 2).

a) Complete helmholtz resonator

b) Decomposition into orifice and backing volume

Fig. 1   Sketch of the considered geometry and reference cut planes 1 and 2 for the decomposed resonator model.
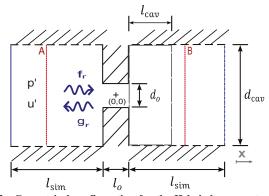
Fig. 2 **Geometrical configuration for the Helmholtz resonator study and boundary conditions: (- - -) slip wall, (—) no-slip wall, (—) prescribed fluctuating velocity, and (-·-) fixed pressure boundary conditions.**

In a general manner, for an incompressible fluid, the momentum equation yields

$$\nabla P = -\rho \frac{\partial \boldsymbol{u}}{\partial t} - \rho(\boldsymbol{\Omega} \times \boldsymbol{u}) + \rho\nu\nabla^2\boldsymbol{u} \qquad (4)$$

where P is the total pressure $P = p + \rho\|\boldsymbol{u}\|^2/2$, where $\boldsymbol{u}$ stands for the velocity, $\boldsymbol{\Omega} = \nabla \times \boldsymbol{u}$ denotes the vorticity, and ρ and ν are the medium density and kinematic viscosity, respectively. The second term on the right-hand side of Eq. (4) is related to the acoustic power in an inviscid and homentropic flow according to Howe's energy corollary [3]. The third term describes the viscous dissipation effects. The total pressure difference ΔP between two sections can be expressed as the sum of two distinct contributions: $\Delta P = \Delta P_{\text{pot}} + \Delta P_s$. The pressure difference ΔP_{pot} is related to a potential flow solution [first term on the right-hand side of Eq. (4)], which would be the solution in the absence of vorticity and viscous effects, whereas ΔP_s is linked to sink/source terms for the sound with both vorticity and viscous effects taken into account [last two terms on the right-hand side of Eq. (4)]. In the numerical models, the viscous dissipation at the walls of the main duct is neglected, and slip boundary conditions are applied. As a consequence, the vorticity and viscous effects can be neglected for the wave propagation in the ducts so that $\Delta P_{\text{duct},s} = 0$ inside the duct segments. In the one-dimensional approximation, ΔP_{pot} can be expressed as

$$\Delta P_{\text{pot}} = -\rho \int_L \frac{\partial u_x}{\partial t}\, \mathrm{d}x \qquad (5)$$

with L the total length between the two sections, x the coordinate along the duct axis, and u_x the axial component of the velocity at the x location (see Fig. 2). Inside the duct segments, $\Delta P_{\text{duct},\text{pot}}$ can be interpreted as a result of the propagation along the duct of the fluctuation in velocity u_x. The pressure losses can be divided spatially between ducts and orifice parts, leading to

$$\Delta P_{AB} = \Delta P_o + \Delta P_{\text{duct}} \;,$$
$$= \Delta P_o + \Delta P_{\text{duct},\text{pot}} + \underset{\nearrow\,0}{\Delta P_{\text{duct},s}} \qquad (6)$$

with ΔP_{AB} the total pressure losses between the measurement sections A and B and ΔP_{duct} the total pressure losses in the two duct segments. From this, the expression to compute the orifice pressure drop ΔP_o is

$$\Delta P_o = \Delta P_{AB} - \Delta P_{\text{duct},\text{pot}} \qquad (7)$$

There are two different ways to determine the orifice transfer impedance values from the measured pressure time series, depending on whether the potential flow pressure loss correction inside the duct is done directly on the pressure time data, or in the frequency domain
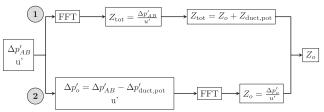

Fig. 3 **Diagram of the two approaches to get the transfer impedance of the orifice from $\Delta p'$: approach 1 (top) and approach 2 (bottom).**

on the impedance itself. Those two approaches to estimate the orifice impedance from the pressure and velocity time series are schematized in Fig. 3.

In approach 1, the impedance due to the duct potential pressure loss $Z_{\text{duct},\text{pot}}$ is subtracted from the total measured impedance Z_{tot} to estimate the transfer impedance from the orifice Z_o as

$$Z_o = Z_{\text{tot}} - Z_{\text{duct},\text{pot}} \qquad (8)$$

For an orifice of thickness l_o placed between the measurement sections A and B, as illustrated in Fig. 2, $Z_{\text{duct},\text{pot}}$ is computed as

$$Z_{\text{duct},\text{pot}} = j\rho\omega(L_{AB} - l_o)u' \qquad (9)$$

where L_{AB} is the distance between the measurement sections A and B, u' is the velocity perturbation inside the duct parts, ω is the angular frequency, and j is the imaginary number $\sqrt{-1}$.

In approach 2, the duct pressure loss is directly subtracted from the time pressure data. As u' does not depend on the position x in the duct segments, one gets

$$\Delta P_{\text{duct}} = \rho(L_{AB} - l_o)\frac{\partial u'}{\partial t} \qquad (10)$$

where $\partial u'/\partial t$ can be computed analytically for harmonic excitation inlet velocity or has to be computed numerically from the velocity time series in case of broadband excitation.

2. Backing Volume Impedance Z_{bc}

The contribution of the backing volume can also be described in terms of a surface impedance $Z_{\text{bc}} = \hat{p}'_1/\hat{u}'_2$, which can be determined through an analytical model. Two analytical expressions for the backing volume are shown here. Using the one-dimensional acoustic equations, the impedance is given as

$$Z_{\text{bc}} = -j\cot(kl_{\text{cav}})\rho c \qquad (11)$$

where k denotes the wave number $k = \omega/c$, c is the speed of sound in the medium, and l_{cav} is the length of the backing cavity. When the whole volume is compressed and expanded simultaneously, the following expression for the impedance can be derived using the isentropic compressibility $\beta \equiv 1/(\rho c^2)$:

$$Z_{\text{bc}} = -j\frac{\rho c^2 S_{\text{bc}}}{V\omega} \qquad (12)$$

This is the same formulation as in, e.g., Keller and Zauner [8]. Both Eqs. (11) and (12) describe the same behavior for $l_{\text{cav}} \ll \lambda_a$. This can be observed by means of the Laurent series of Eq. (11): $Z_{\text{bc}}/(\rho c) = -i[1/(kl_{\text{cav}}) - kl_{\text{cav}}/3 - k^3 l^3_{\text{cav}}/45 + \mathcal{O}(k^5 l^5_{\text{cav}})]$. The first term of the expansion is identical to the expression in Eq. (12). Note that both expressions deliver a purely reactive contribution from the backing cavity. Equation (12) is used in the present study.

B. Case Configuration and Numerical Setup

The geometric configuration for the incompressible simulations as well as the definition of the boundary conditions for the unsteady CFD are illustrated in Fig. 2. The numerical domain consists of an orifice of

diameter $d_o = 4.2$ mm and thickness $l_o = 4.0$ mm, placed in a duct of diameter $d_{cav} = 50$ mm. This gives a porosity σ of the resonator front plate of 0.71%. Those dimensions have been chosen according to the Ref. [9], corresponding to the case with sharp edges, used for comparison (see Sec. II.C). The original resonator design has a cavity length of $l_{sim}/d_{cav} = 0.4$. The extension of the computational domain in the axial direction l_{sim} should be long enough to allow measurement sections to be put out of the area that is influenced by hydrodynamic fluctuations. For the investigated case described through this work, l_{sim}/d_{cav} equals 10 and has been taken long to allow different measurement sections at $x/d_{cav} = [\pm 8, \ \pm 6, \ \pm 4, \ \pm 2]$ along the duct for assessment of the methodology. Numerically determined impedance results have been shown independent of the location of the chosen measurement sections after post-processing. This ensures that the impedance results are not polluted due to vortices crossing the measurement sections. The length $l_{sim}/d_{cav} = 2$ has been found to be sufficient for the investigated geometry at the investigated SPLs, and it reduces considerably the computational cost and time.

Figure 2 presents also the boundary conditions used for the unsteady incompressible CFD computations. The wall of the duct is defined as the slip-wall boundary condition. This assumption implies that no boundary layer develops along the duct and that the velocity profile is constant through the section. Such a hypothesis is fair, as it has been observed in various compressible studies, e.g., the large-Eddy simulation (LES) computations performed by Alenius [10], that changing this boundary condition does not affect the local orifice behavior. This assumption is of importance for the present study, as it allows one to easily discard pressure losses occurring in the duct upstream and downstream of the orifice. The wall of the orifice plate is, however, prescribed as no-slip boundary condition as the resolution of the boundary layers in the vicinity of the orifice is of major importance for a correct orifice impedance estimation. The velocity is prescribed at the duct inlet boundary as a time-dependent harmonic fluctuation with zero mean. Finally, a fixed pressure boundary condition is applied to the outlet side of the duct to close the problem definition.

The present approach is limited to cases in which the hydrodynamic vortex structures are contained inside the numerical domain. As the boundary conditions for the incompressible simulations are defined through prescribed velocity and pressure values, vortices crossing the domain limits are not accounted for by boundary treatment. Violation of this rule has shown to deliver inaccurate results as the numerical problem formulation is inconsistent in that case. If vortices approach the in-/outflow boundaries, the computational domain has to be extended. This can be required for configurations with orifices of small diameter at high excitation amplitudes, as for those cases the vortices can travel far away from the production zone.

In this work, the incompressible finite-volume solver of a commercial code (ANSYS Fluent v14/v15) is used to characterize the flow. The chosen solver is pressure based, time-dependent, implicit, and second order in time and space. The pressure correction scheme applied is Semi-Implicit Method for Pressure-Linked Equations. No turbulence modeling is applied for the presented simulation results as the Reynolds number based on the orifice size and velocity fluctuation amplitude at the orifice is rather low (maximum $Re \approx 3000$ at high excitation levels). Turbulence modeling has shown very limited impact on the estimated orifice transfer impedance under the present operating conditions. Comprehensive parameter studies regarding grid, time step, and solver parameters have been performed to ensure that the presented results are independent of those numerical settings. Standard parameters for the results presented here are the minimal size of mesh cell $h_{min} = 10^{-5}$ m, time step $dt = 10^{-6}$ s, number of iterations per time step $N_{iter} = 20$. Both two-dimensional axisymmetric and three-dimensional simulations have been carried out in this work to investigate three-dimensional effects.

C. References for Validation of Method

As mentioned in Sec. I, the results computed from incompressible unsteady CFD simulations are compared to two different data sets: compressible CFD results and experimental data performed on a

particular Helmholtz resonator geometry. This paragraph describes briefly those references and the geometric definition of this particular case. More detailed on the reference works can be found in the papers [9,11].

1. Numerical Compressible Computational Fluid Dynamics Reference Data

Compressible simulations of the Navier–Stokes equations with both laminar and turbulent models (LES with the k-equation eddy-viscosity model) performed with the Pimple algorithm of OpenFOAM [12] are used for comparison [9,11]. To distinguish, for the estimated resonator acoustic impedance, between the possible differences originating from the numerical solvers and from the modeling part, both open-end tube (without accounting for the cavity backing wall) and closed-end tube (Helmholtz resonator) configurations are simulated with the compressible solver. It was also verified that the turbulence modeling leads only to very minor differences. With the turbulence model activated, the acoustic resistance increased slightly. This shows that turbulent structures as represented by the subgrid scale model do not have a significant impact on the separation mechanism itself in the chosen SPL range.

In the compressible flow simulations, the computational domain is excited from the boundary opposite to the resonator at a distance $l_{sim}/d_{cav} = 2$ by imposing a propagating characteristic wave F_r of amplitude A_f. For this purpose, the Navier–Stokes characteristics boundary condition, cf. Poinsot and Lele [13], is applied. Particular care has been taken to match A_f with the value of the amplitude A_u in the incompressible flow simulations to ensure the same excitation state of the orifice in both closed and open tubes. The method to define correctly the excitation amplitude is discussed in detail in Sec. II.D. The F_r wave can be imagined as a wave traveling in the right direction toward the orifice location, whereas G_r is the reflected one traveling back to the inlet. Shortly after the inlet, area-averaged pressure and velocity fluctuations were evaluated across a reference plane to determined F_r and G_r time series to evaluate the reflection coefficient R_{num}. For those harmonically excited simulations, the reflection coefficient is determined through $R_{num}(\omega) = \hat{g}_r(\omega)/\hat{f}_r(\omega)$, with angular frequency ω. The reflection coefficient is transformed to the resonator normalized surface impedance z_r, using the relation $z_r = (1 + R_{num/exp})/(1 - R_{num/exp})$.

2. Experimental Reference Data

In addition to the numerical results, a measurement campaign has been performed by Förner et al. [9] at the Eindhoven University of Technology on a Helmholtz resonator configuration. The experiments were carried out with an impedance tube in a semi-anechoic chamber. The resonator sample was placed at one extremity of the impedance tube. The measurement data give the surface impedance of the complete Helmholtz resonator. The tube has six BSWA MPA416 microphones with the average sensitivity of 50.45 mV/Pa, equally distributed along the 1-m-long tube. The microphones have been calibrated to measure the reflection coefficient R_{exp} in the frequency range [100–700 Hz]. The numerical work will limit itself to this frequency range. The reflection behavior of the test object has been studied for various SPLs. Data for the cases 89.3 and 119.7 dB are presented here for assessment of the investigated methodology. Those SPL values are controlled over the entire frequency range at a reference position, here the closest microphone from the resonator front plate placed 49.7 mm away. The 89.3 dB case is in the linear regime, while in the 119.7 dB case, nonlinearities are present.

D. Setting Excitation Amplitudes

For the purpose of comparing results of the incompressible simulations with existing experimental data, it is necessary to ensure that the velocities in the orifice agree with each other for the different setups. This fact is also relevant for comparison with the compressible solver, as the definition of the excitation between compressible and incompressible solvers is fundamentally different. The excitation is given by a time-varying axial velocity fluctuation at the inlet boundary for the incompressible simulations, whereas it is

defined through injection of an F_r wave for the compressible ones. The reflection coefficient is therefore a key parameter to match results in the nonlinear regime. This has been found to be a challenge from a practical point of view. Drawing impedance curves from a particular resonator at a certain SPL given at a reference position can also be achieved by the present incompressible approach without any knowledge of intermediate variables such as the reflection coefficient. This requires, nevertheless, in general, several simulation trials for one case, in which the input velocity is progressively modified until the SPL matches the target one.

To compare the results from the investigated methodology to existing data sets, the following procedure has been applied, based on the relations between propagating waves F_r and G_r and primitive variables p' and u'. Below the cut-off frequency of the duct, and in the case of no mean flow, the acoustics can be described as the superposition of the Riemann invariants defined by $F_r = 1/2(p'/(\rho c) + u')$ and $G_r = 1/2(p'/(\rho c) - u')$. In the resonance tube, a standing wave is developed with a fluctuating pressure at the position x,

$$p'(x) = \rho c[F_r(x) + G_r(x)] \tag{13}$$

In the experimental setup, the reference microphone was mounted at a distance of $l_{ref} = 0.0497$ m away from the resonator front face. This is selected as the reference position x_{ref} for the SPL. Moreover, the reflection coefficient $R = G_r/F_r$ depends on both frequency and amplitude. The reflected wave at the reference position is thus $G_r(x_{ref}) = R(\omega, \text{SPL})\exp(-j\omega 2l_{ref}/c)F_r(x_{ref})$. Accordingly, the fluctuating pressure at position x_{ref} is given as $p'/(\rho c) = [1 + R(\omega, \text{SPL})\exp(-j\omega 2l_{ref}/c)]F_r(x_{ref})$. Considering the ratio of rms values to harmonic amplitude being $1/\sqrt{2}$, the amplitude A_f of the incoming wave $F_r = A_f \exp(j\omega t)$ is given as

$$A_f = 10^{\text{SPL}/20}\frac{\sqrt{2}p_a}{|1 + R(\omega, \text{SPL})\exp(-j\omega 2l_{ref}/c)|\rho c} \tag{14}$$

where $p_a = 20$ μPa is the commonly used reference sound pressure in air.

The fluctuating velocity u' is given as the difference of the Riemann invariants, i.e., $u' = F_r - G_r$. Thus, the amplitude of the velocity A_u at the resonator mouth position (at $x_o = -l_o/2$ in this work) can be calculated as

$$A_{u(x_o)}(\omega, \text{SPL}) = A_f(\omega, \text{SPL})|1 - R(\omega, \text{SPL})| \tag{15}$$

For the incompressible simulations, the inlet amplitude prescribed at the inlet boundary is directly given by Eq. (15). For the compressible simulations, in the case of the full resonator configuration, the inlet boundary condition is A_f given by Eq. (14). Finally, exchanging the backing cavity with a nonreflecting outlet ($Z = \rho c$), the amplitude of the F_r wave has to be corrected. The reflection coefficient of the corresponding orifice R_o (i.e., open tube) can be estimated as

$$R_o = \frac{z_r - z_{bc}}{z_r - z_{bc} + 2} \tag{16}$$

Thus, the amplitude of the i wave in the open-end tube configuration $A_{f,o}$ should be set as

$$A_{f,o} = A_f\frac{|1 - R|}{|1 - R_o|} \tag{17}$$

Table 1 lists the values of the different excitation amplitudes needed to ensure the same state at the orifice neck for five frequencies close to the resonator eigenfrequency and for the two investigated SPLs. As the primitive variables and Riemann variables are linked through the reflection coefficient, values of velocity at the orifice coming from the compressible simulations are still slightly different, but these deviations have been judged to have only a small impact on

Table 1 Example of inlet excitation amplitudes for F_r and u' at two different SPLs

Frequency, Hz	340	360	380	400	420
	SPL = 89.3 dB				
A_f, m/s	0.0020	0.0033	0.0019	0.0013	0.0011
A_u, m/s	0.0021	0.0043	0.0024	0.0014	0.0009
$A_{f,o}$, m/s	0.0076	0.0165	0.0097	0.0057	0.0041
	SPL = 119.7 dB				
A_f, m/s	0.0552	0.0601	0.0574	0.0490	0.0401
A_u, m/s	0.0411	0.0474	0.0471	0.0407	0.0295
$A_{f,o}$, m/s	0.1500	0.1823	0.1891	0.1693	0.130

the estimated impedance values. Note that in the linear regime (here at 89.3 dB), even if specific values are given in Table 1, computations give the same impedance values taking different inlet velocity amplitudes, as long as these prescribed excitation amplitudes are small enough to remain in the linear regime of the resonator.

III. Results Obtained for Small Excitation Amplitudes: Linear Regime

For harmonic pulsating flows at the orifice, the impedance value for each excitation frequency is computed by dividing the Fourier coefficients of the fluctuating pressure loss through the orifice $\Delta\hat{p}'$ with the velocity perturbation $\hat{u}'$. Each frequency requires therefore one CFD simulation. The harmonic fluctuating inlet velocity is given for a given angular frequency ω by

$$u'(t) = A_u \sin(\omega t) \tag{18}$$

where the amplitude of inlet velocity A_u is defined as described in Sec. II.D.

A. Resonator Impedance in Linear Regime

Figure 4 shows the obtained normalized surface impedance curves for the case SPL = 89.3 dB over the frequency range [100–700 Hz] compared to the experimental data and the values obtained from the system identification of the complete three-dimensional resonator model with the compressible solver. Impedance values are normalized by the characteristic isentropic impedance $Z_0 = \rho c$. For each simulation set, it is verified that the impedance values are independent of the measurement sections selected for determining the pressure loss.

All results show a fair agreement around the Helmholtz resonance frequency $f_{H,lin} = 372$ Hz in the linear regime. The reactance $Im(z_r)$ matches well with the experimental data over the entire frequency range. However, one can see that the discrepancies increase slightly with increasing frequency. The incompressible harmonic results lead to a better reactance prediction than the compressible solver far from the resonator eigenfrequency. The same observation can be made on the resistance $Re(z_r)$. Notice also that both experimental and compressible values present a large error far from the resonance frequency as the impedance values are obtained using the reflection coefficient R_{exp} or R_{num}, so that even a small error on the reflection coefficient gives a larger uncertainty on the impedance in such a condition. This comes from the fact that the transformation from $R_{exp/num}$ to $Re(z_r)$ is ill conditioned away from the eigenfrequency in the case of the complete Helmholtz resonator, as the magnitude of the reflection coefficient is close to unity at these frequencies. The resistance obtained by incompressible simulations seems a bit lower than experimental data, but the trend in frequency (given by the slope) is well predicted.

B. Comparison of Two Approaches in Harmonic Case

The two approaches to extract Z_o from the incompressible results, as discussed in Sec. II.A, are investigated here in the case of the linear regime with harmonically excited resonator. The difference in concept between those approaches lies in the correction of the
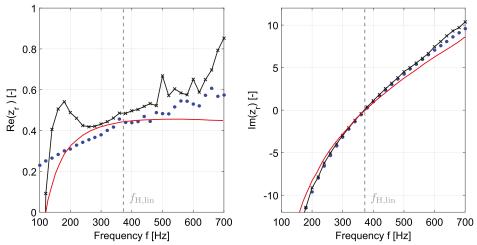
Fig. 4 Normalized resistance $Re(z_r)$ (left) and reactance $Im(z_r)$ (right) of the Helmholtz resonator, obtained with the methodology based on incompressible simulations, compared to experimental data and broadband compressible numerical results (case SPL = 89.7 dB): (●) two-dimensional incompressible, (——) three-dimensional compressible with broadband excitation, and (-×-) experimental data.
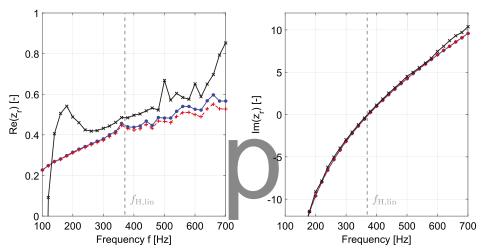

Fig. 5 Normalized resistance $Re(z_r)$ (left) and reactance $Im(z_r)$ (right) of the Helmholtz resonator evaluated from incompressible simulations with the approaches 1 and 2: (-●-) approach 1, (-+-) approach 2, and (-×-) experimental results.

pressure losses in the duct segments: in the frequency domain (approach 1) or in the time domain (approach 2). Figure 5 shows that there is a good agreement between impedance values resulting from both approaches. The reactance values in particular are very similar. More discrepancies can be noticed on the resistive part of the impedance with the difference between the approaches growing when the frequency is increasing. It was observed that approach 2 is more sensitive to the simulation parameters (time step, mesh refinement, and dependency of the measurement section) than approach 1, but both approaches converge to the same impedance values. Approach 1 can therefore be favored for its robustness. Those conclusions drawn for the linear regime with harmonic signal excitation have been verified to be valid for the nonlinear regime and for the linear regime with broadband excitation as well.

IV. Results Obtained for Higher Excitation Amplitudes

This section presents the results obtained for higher excitation amplitudes, where flow separates at the edges of the orifice, i.e., in the nonlinear resonator regime.

A. Resonator Impedance in Nonlinear Regime

Figure 6 presents the normalized impedance obtained at a SPL of 119.7 dB from the different numerical methods performed on the investigated resonator geometry compared to the experimental data. Three-dimensional simulations have been performed with a much

shorter computational domain with $l_{sim}/d_{cav} = 2$. The three-dimensional mesh consists of nearly 1.5 million cells. Impedance results from different measurement sections have been shown to be identical.

The main conclusion from this work is that the tested numerical models, in spite of their differences in terms of physics and methodology, are in very good agreement. Nevertheless, a systematic overprediction of the resistance compared to experimental results can been seen. The discrepancy is expected to be of physical nature, as mesh/time-step influences have been discarded. The reason for this discrepancy is still under investigation. The comparison of the results for the whole resonator and the results obtained by simulating separately the orifice and the back cavity shows overall that the combined model gives very satisfying results and that this model is still valid for this range of moderately high sound amplitudes. Some small differences between the two- and three-dimensional models can be observed, but the overall impact of three-dimensional effects is rather small, although it clearly increases with increasing velocity at the orifice. The flow visualization (not shown here) suggests that the eddies dissipate in an asymmetrical manner but that this asymmetry does not influence the separation process itself. Thus, the three-dimensional effects are not important from an acoustical point of view for the considered SPLs. For the reactance, numerical and experimental data are very similar, with a very good match of all numerical results. In detail, it seems, however, that the numerical approaches underpredict to some very small extent the reactance,
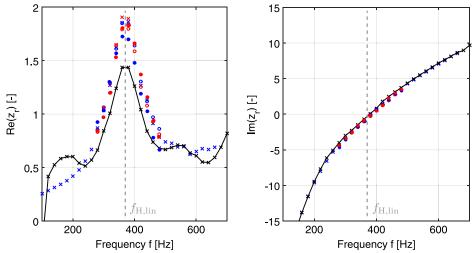
Fig. 6 Comparison of numerical results from the different solvers with experimental data for the case at 119.7 dB: (-×-) experimental results [9], (×) two-dimensional incompressible decomposed model, (○) two-dimensional compressible decomposed model, (●) two-dimensional full resonator, (×) three-dimensional incompressible decomposed model, (○) three-dimensional compressible decomposed model, and (●) three-dimensional full resonator.

giving a slightly higher resonance frequency. When compared to the previous linear regime case, one can note that the reactance is only in a minor way affected by variation of the excitation amplitude.

Complementary computations have been run for a different Helmholtz resonator geometry, based on the case studied by Hersh et al. [14] (see Fig. 12a in the referred work), to see if the overprediction in resistance is also present. For this second resonator geometry, the dimensions of the acoustic resonator are $l_o = 1.59$ mm, $d_o = 6.35$ mm, $l_{cav} = 25.4$ mm, and $d_{cav} = 50.8$ mm. Figure 7 shows the comparison of the numerical results from both incompressible and compressible numerical approaches to the experimental data of the literature. The general trends for both resistive and reactive parts with respect to increasing excitation amplitudes are correctly captured by the numerical methods. A good quantitative agreement is also obtained. A shift in the resonance frequency can be clearly observed in Fig. 7, with a growing deviation from its value in the linear regime $f_{H,lin}$ toward higher frequencies for increasing SPLs. This shift occurs due to a decrease of the reactance for increasing excitation amplitudes, which is related to a reduction of the effective length by vortex shedding [15]. Since the neck geometric length is smaller in this case than for the first resonator configuration investigated, this effect is much more visible here. The present cases correspond to high Strouhal numbers $Sh \gg 1$, with $Sh \in [25{-}60]$, where $Sh = d_o \sqrt{\omega \rho/(4\mu)}$ is the ratio of the Stokes layer thickness to the orifice diameter. The physical interpretation of the nonlinear impedance at such high Shear number values was shown [15] to be

more complicated than at smaller Sh, due to complex vortex shedding effects, and requires further investigation. The resistance over-prediction from the numerical methods seems to be still present in this case, even if significantly less pronounced.

B. Effects of Rounded Edges

One possible reason for the systematic difference between experimental and numerical impedance results has been thought to originate from the existence of some rounding of the edges for the experimental Helmholtz resonator test sample. It was already shown in previous works [9,16] that the presence of chamfers strongly changes the structures of the produced vortices and the resistance at moderate and high excitation amplitudes. In the present study, the size of the considered chamfers is much smaller so that one can speak about microchamfers or microrounded edges. These microrounded edges are investigated as representing more realistic edges, similarly to the ones expected from manufacturing processes.

Figure 8 shows the impact of microrounded edges on the impedance for both linear and nonlinear regimes. In the linear regime, the microrounded edges affect neither the determined resistance nor reactance. This is expected as the volume of the orifice is not considerably modified by the microchamfering and therefore the reactance, related to the inertial effects, is not altered. The geometrical modification at the orifice edges does not influence the flowpath, producing no change for the pressure drop and therefore no change in the resistance, either. In the nonlinear regime, one can
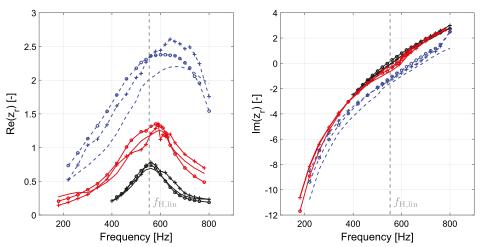

Fig. 7 Normalized resistance $Re(z_r)$ (left) and reactance $Im(z_r)$ (right) for the Hersh Helmholtz resonator configuration at three SPLs (—) 120 dB, (—) 130 dB, and (- - -) 140 dB, obtained from the (-+-) incompressible method, (-○-) compressible method, and (—) experimental data from Hersh [14].

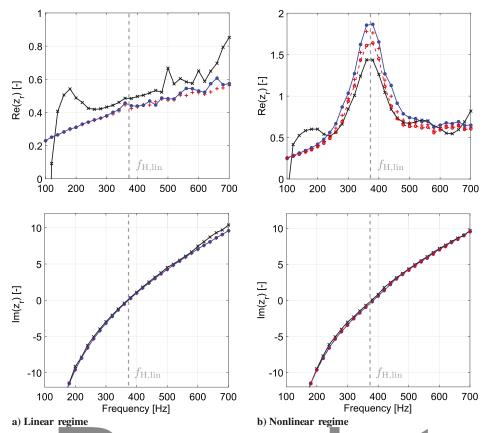**a) Linear regime**   **b) Nonlinear regime**

Fig. 8   Impact of edge rounding on the computed Helmholtz resonator impedance for the configuration described in Sec. II.B, in the a) linear and b) nonlinear regimes: (-●-) sharp edges incompressible, (-×-) experimental data, (+) $R_f = 40\ \mu m$ rounded edges incompressible, and (-○-) $R_f = 80\ \mu m$ rounded edges incompressible.

observe from Fig. 8 that even small microrounded edges can affect significantly the predicted resistance values. Results for two different rounded edge radii are shown, $R_f = 40\ \mu m$ and $R_f = 80\ \mu m$, respectively. These radii represent 1 and 2% of the orifice thickness. From those observations, accounting for rounded edges tends to decrease the resistance, delivering a better agreement with the experimental results. After consideration of the rounded edge radius for the actual test sample, which is found to be close to 80 μm, the extent of this change for the present case seems, however, to not fully explain the observed discrepancies in resistance between the numerical and experimental approaches. A rounded edge radius lager than 120 μm would indeed be required in the simulations to equal the experimental resonance peak in resistance. No impact on the reactance can be noticed. Additional flow computations have shown that the impact of rounded edges on the impedance is captured in a similar manner for both compressible and incompressible cases, for both rounded edges and straight chamfer situations. The actual microscale geometry does not change the results significantly.

V.   Conclusions

A method to numerically characterize the aeroacoustic behavior of Helmholtz resonators without mean flow has been investigated. Both linear and nonlinear regimes have been studied. A procedure to assess the present methodology, by ensuring the same velocities in the orifice as in compressible flow simulations and experiments, is described in this paper. The impedance values obtained with the incompressible computational fluid dynamics (CFD) simulation of the orifice combined with an analytical backing volume model are in good agreement with results from a compressible simulation of a complete resonator. The numerical results for the resistance in the nonlinear regime show a systematic overprediction with respect to experimental data. The impact of microrounded edges on the estimated impedance has been investigated. Even if the presence of microrounded edges was deemed insufficient to explain alone the

discrepancies, such geometrical details were found to affect significantly the computed resonator resistance and should therefore be included for accurate predictions of the acoustic behavior of Helmholtz resonators in their nonlinear regime.

The presented approach has shown, nevertheless, to give satisfying results for the acoustic impedance of Helmholtz resonators. It is an alternative for the study of the nonlinear regime of such acoustic damping systems. The proposed methodology can be applied for the study of both linear and nonlinear regimes of the Helmholtz resonator with commercial CFD software with moderate computational costs. One of the most significant advantages of this methodology is that it does not rely on the reflection coefficient to estimate the impedance (as in experiments or compressible simulations) and instead the impedance is directly computed from the pressure and velocity. Impedance curves are therefore valid on a broader frequency range than just around the resonator resonance frequency. This approach can be extended to the study of an orifice with bias or grazing flow in a straightforward manner following previous works [2,4,6]. In the no-mean-flow case, two possible approaches in the postprocessing of the orifice transfer impedance have been studied. The difference in concept between those approaches lies in the correction of the pressure losses in the duct segments: in the frequency domain (approach 1) or in the time domain (approach 2). A general conclusion is that both approaches investigated in this work lead to similar impedance prediction, but approach 1 has been shown to be more robust. Finally, the possible impact of three-dimensional effects on the impedance results presented in this work has been investigated and judged minor for the applied conditions.

References

[1] Denayer, H., Tournadre, J., De Roeck, W., Desmet, W., and Martínez-Lera, P., "Combined Numerical and Experimental Study of a Slit Resonator Under Grazing Flow," *Proceedings of the 20th AIAA/CEAS Aeroacoustics Conference*, AIAA Paper 2014-2959, 2014.

[2] Martínez-Lera, P., Schram, C., Föller, S., Kaess, R., and Polifke, W., "Identification of the Aeroacoustic Response of a Low Mach Number Flow Through a T-Joint," *Journal of the Acoustical Society of America*, Vol. 126, No. 2, 2009, pp. 582–586.
doi:10.1121/1.3159604

[3] Howe, M. S., "Theory of Vortex Sound," *Cambridge Texts in Applied Mathematics*, Cambridge Univ. Press, Cambridge, England, U.K., 2003, pp. 114–132.

[4] Nakiboğlu, G., Belfroid, S. P. C., Golliard, J., and Hirschberg, A., "On the Whistling of Corrugated Pipes: Effect of Pipe Length and Flow Profile," *Journal of Fluid Mechanics*, Vol. 672, No. 1, 2011, pp. 78–108.
doi:10.1017/S0022112010005884

[5] Lacombe, R., Moussou, P., and Aurégan, Y., "Identification of Whistling Ability of a Single Hole Orifice from an Incompressible Flow Simulation," *Proceedings of the ASME, Pressure Vessels and Piping Conference, Fluid-Structure Interaction*, Vol. 4, ASME Paper PVP2011-57355, 2011, pp. 261–267.
doi:10.1115/PVP2011-57355

[6] Golliard, J., González-Díez, N., Belfroid, S., Nakiboğlu, G., and Hirschberg, A., "U-RANS Model for the Prediction of the Acoustic Sound Power Generated in a Whistling Corrugated Pipe," *Proceedings of the ASME, Pressure Vessels and Piping Conference, Fluid-Structure Interaction*, Vol. 4, ASME Paper PVP2013-97385, Paris, France, July 2013, Paper V004T04A040.
doi:10.1115/PVP2013-97385

[7] Ingard, U., and Ising, H., "Acoustic Nonlinearity of an Orifice," *Journal of the Acoustical Society of America*, Vol. 42, No. 1, 1967, pp. 6–17.
doi:10.1121/1.1910576

[8] Keller, J., and Zauner, E., "On the Use of Helmholtz Resonators as Sound Attenuators," *Journal of Applied Mathematics and Physics*, Vol. 46, No. 3, 1995, pp. 297–327.
doi:10.1007/BF01003552

[9] Förner, K., Temiz, M. A., Polifke, W., Arteaga, I. L., and Hirschberg, A., "On the Non-Linear Influence of the Edge Geometry on Vortex Shedding in Helmholtz Resonators," *Proceedings of the 22nd International Conference on Sound and Vibration*, The International Inst. of Acoustics and Vibration (IIAV) and the Acoustical Soc. of Italy (AIA) Paper 2015-1341, 2015.

[10] Alenius, E., "Flow Duct Acoustics: An LES Approach," Ph.D. Thesis, Royal Inst. of Technology, Stockholm, Sweden, 2012.

[11] Förner, K., and Polifke, W., "Aero-Acoustic Characterization of a Helmholtz Resonator in the Linear Regime with System Identification," *Proceedings of the 22nd International Conference on Sound and Vibration*, The International Inst. of Acoustics and Vibration (IIAV) and the Acoustical Soc. of Italy (AIA) Paper 2015-596, 2015.

[12] "OpenFOAM (Open Field Operation and Manipulation)," Software Package Ver. 2.3.0, OpenFOAM Foundation, London, U.K., Feb. 2014.

[13] Poinsot, T. J., and Lele, S. K., "Boundary Conditions for Direct Simulations of Compressible Viscous Flows," *Journal of Computational Physics*, Vol. 101, No. 1, 1992, pp. 104–129.
doi:10.1016/0021-9991(92)90046-2

[14] Hersh, A. S., Walker, B. E., and Celano, J. W., "Helmholtz Resonator Impedance Model, Part 1: Nonlinear Behavior," *AIAA Journal*, Vol. 41, No. 5, 2003, pp. 795–808.
doi:10.2514/2.2041

[15] Temiz, A. M., Tournadre, J., Lopez-Artega, I., and Hirschberg, A., "Non-Linear Acoustic Transfer Impedance of Micro-Perforated Plates with Circular Orifices," *Journal of Sound and Vibration*, Vol. 366, No. 1, 2016, pp. 418–428.
doi:10.1016/j.jsv.2015.12.022

[16] Laudien, E., Pongratz, R., Pierro, R., and Preclik, D., "Fundamental Mechanisms of Combustion Instabilities: Experimental Procedures Aiding the Design of Acoustic Cavities," *Liquid Rocket Engine Combustion Instability*, AIAA, Washington, D.C., 1995, pp. 377–399.

P. G. Tucker
Associate Editor